

Towards Certified Robustness of Metric Learning

Xiaochen Yang^{*1}, Yiwen Guo^{*2}, Mingzhi Dong¹, and Jing-Hao Xue^{†1}

¹Department of Statistical Science, University College London, London WC1E 6BT, UK.

²Bytedance AI Lab, Beijing 100000, China.

Abstract

Metric learning aims to learn a distance metric such that semantically similar instances are pulled together while dissimilar instances are pushed away. Many existing methods consider maximizing or at least constraining a distance “margin” that separates similar and dissimilar pairs of instances to guarantee their performance on a subsequent k -nearest neighbor classifier. However, such a margin in the *feature* space does not necessarily lead to robustness certification or even anticipated generalization advantage, since a small perturbation of test instance in the *instance* space could still potentially alter the model prediction. To address this problem, we advocate penalizing small distance between training instances and their nearest adversarial examples, and we show that the resulting new approach to metric learning enjoys a larger certified neighborhood with theoretical performance guarantee. Moreover, drawing on an intuitive geometric insight, the proposed new loss term permits an analytically elegant closed-form solution and offers great flexibility in leveraging it jointly with existing metric learning methods. Extensive experiments demonstrate the superiority of the proposed method over the state-of-the-arts in terms of both discrimination accuracy and robustness to noise.

1 Introduction

Distance metric learning (DML) focuses on learning similarity or dissimilarity between data and it has been actively researched in classification and clustering [47, 18, 3], as well as domain-specific applications such as information retrieval [27, 46], computer vision [17, 14, 30] and bioinformatics [42]. A commonly studied distance metric is the generalized (squared) Mahalanobis distance, which defines the distance between any two instances $\mathbf{x}_i, \mathbf{x}_j \in \mathbb{R}^p$ as

$$d_M^2(\mathbf{x}_i, \mathbf{x}_j) = (\mathbf{x}_i - \mathbf{x}_j)^T \mathbf{M}(\mathbf{x}_i - \mathbf{x}_j),$$

where \mathbf{M} is a positive semidefinite (PSD) matrix. Owing to its PSD property, \mathbf{M} can be decomposed into $\mathbf{L}^T \mathbf{L}$ with $\mathbf{L} \in \mathbb{R}^{d \times p}$; thus the Mahalanobis distance is equivalent to the Euclidean distance $\|\mathbf{L}\mathbf{x}_i - \mathbf{L}\mathbf{x}_j\|_2^2$ in the linearly transformed feature space. When $d < p$, instances \mathbf{x}_i and \mathbf{x}_j are transformed from a high-dimensional instance space to a low-dimensional feature space.

To learn a specific distance metric for each task, prior knowledge on instance similarity and dissimilarity should be provided as side information. Metric learning methods differ by the form of side information they use and the supervision encoded in similar and dissimilar pairs. For example, pairwise constraints enforce the distance between instances of the same class to be small (or smaller than a threshold value) and the distance between instances of different classes to be large (or larger than a threshold value) [41, 40, 38, 9, 13]. The thresholds could be either pre-defined or learned for similar and dissimilar pairs [7, 19]. In triplet constraints $(\mathbf{x}_i, \mathbf{x}_j, \mathbf{x}_l)$, distance between the different-class pair $(\mathbf{x}_i, \mathbf{x}_l)$ should be larger than distance between the same-class pair $(\mathbf{x}_i, \mathbf{x}_j)$, and typically, plus a margin [39, 33, 44, 24]. More recently, quadruplet constraints are proposed, which require the difference in the distance of two pairs of instances to exceed a margin [20], and $(N + 1)$ -tuple extends the triplet constraint for multi-class classification [32, 22].

^{*}Equal contribution

[†]Corresponding author; Email address: jinghao.xue@ucl.ac.uk

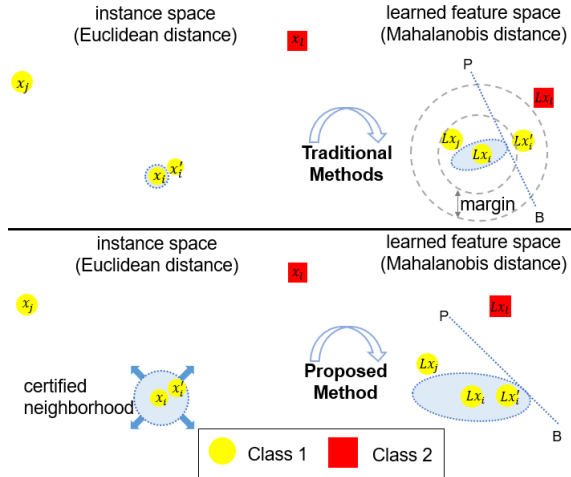


Figure 1: Comparison of traditional metric learning methods and the proposed method. While classical methods separate similar and dissimilar pairs by a margin (indicated by the gap between gray dashed circles), a small perturbation from \mathbf{x}_i to \mathbf{x}'_i in the instance space may change its nearest neighbor (NN) from \mathbf{x}_j to \mathbf{x}_l in the learned feature space. Our method aims to expand a certified neighborhood (indicated by blue dotted circle), defined as the largest hypersphere in which \mathbf{x}_i could be perturbed without any label change on its NN in the learned feature space. Points on line PB are equidistant from \mathbf{x}_j and \mathbf{x}_l with respect to the learned distance.

The gap between thresholds in pairwise constraints and the margin in triplet and quadruplet constraints are both designed to learn a distance metric that could ensure good generalization of the subsequent k -nearest neighbor (NN) classifier. However, such a separating margin imposed at the distance and decision level does not necessarily produce a robust metric – indeed it may be sensitive to a small perturbation at the instance level. As illustrated in Fig. 1 (upper), a tiny perturbation from \mathbf{x}_i to \mathbf{x}'_i in the instance space can be magnified by the learned distance metric, leading to a change in its NN from \mathbf{x}_j to \mathbf{x}_l in the feature space, and even worse, an incorrect label prediction if 1-NN is used.

In this paper, we propose a simple yet effective method to enhance robustness of the learned distance metric against instance perturbation. The principal idea is to expand a *certified neighborhood*, defined as the largest hypersphere in which a training instance could be perturbed without changing the label of its nearest neighbor (or k nearest neighbors if required) in the feature space.

Our contributions are mainly fourfold. Firstly, we derive an analytically elegant solution to the radius of certified neighborhood (Sec. 2.1). It is equivalent to the distance between a training instance \mathbf{x}_i and its nearest adversarial example [34] termed *support point*. Building on a geometric insight, the support point can be easily identified as the closest point to \mathbf{x}_i in the instance space that lies on the decision boundary in the feature space. Secondly, we define a new perturbation loss that penalizes the radius for being small, or equivalently, encourages an expansion of certified neighborhood (Sec. 2.1), which can be optimized jointly with any existing triplet-based metric learning methods (Sec. 2.2). The optimization problem suggests that our method learns a discriminative metric in a weighted manner and simultaneously imposes a data-dependent regularization. Thirdly, because learning a distance metric for high-dimensional data may suffer from overfitting, we extend the perturbation loss so that the metric could be learned based on PCA transformed data in a low-dimensional subspace while retaining the ability to withstand perturbation in the original high-dimensional instance space (Sec. 2.3). Fourthly, we show the benefit of expanding a certified neighborhood to the generalization ability of the learned distance metric by using the theoretical technique of algorithmic robustness [43] (Theorem 3, Sec. 2.4). Experiments in noise-free and noisy settings show that the proposed method outperforms existing robust metric learning methods in terms of classification accuracy and validate its robustness to noise (Sec. 3).

Related work To improve robustness to perturbation that is likely to exist in practice, many robust metric learning methods have been proposed, which can be categorized into three main types. The first type of methods imposes structural assumption or regularization over \mathbf{M} so as to avoid overfitting [16, 23, 37, 21, 15, 26, 25]. However, structural information often exists in image datasets but is generally unavailable in the symbolic datasets studied in this paper. Regularization-based methods are proposed to reduce the risk of overfitting to feature noise. Our proposal, which is aimed to withstand perturbation, does not conflict with these methods and can be combined with them to learn a more effective and robust distance metric; an example is shown in Sec. 3.2. The second type of methods explicitly models the perturbation distribution or identifies clean latent examples [48, 29]. The expected Mahalanobis distance is then used to adjust the value of separating margin. The third type of methods generates hard instances through adversarial perturbation and trains a metric to fare well in the new hard problem [6, 11]. Although

sharing the aim of improving metric robustness, these methods approach the task at a data-level by synthesizing real examples that incur large losses, while our method tackles perturbation at a model-level by designing a loss function that considers the definition of robustness with respect to the decision maker k NN. By preventing change in the nearest neighbor in a strict manner, our method can obtain a certification on the adversarial margin. Finally, we note that a large margin in the instance space has been studied in deep neural networks for enhancing robustness and generalization ability [1, 12, 45, 8]. In contrast, our paper investigates such margin in the framework of metric learning, defines it specifically with respect to the NN classifier, and provides an exact and analytical solution to the margin.

Notation Let $\{\mathbf{x}_i, y_i\}_{i=1}^n$ denote the set of training instance and label pairs, where $\mathbf{x}_i \in \mathcal{X} \subseteq \mathbb{R}^p$ and $y_i \in \mathcal{Y} = \{1, \dots, C\}$; \mathcal{X} is called the instance space in this paper. Our framework is based on triplet constraints $\{\mathbf{x}_i, \mathbf{x}_j, \mathbf{x}_l\}$ and we adopt the following strategy for generating triplets [39]:

$$\begin{aligned} \mathcal{S} &= \{(\mathbf{x}_i, \mathbf{x}_j) : \mathbf{x}_j \in \{k\text{NNs with the same class label of } \mathbf{x}_i\}\}, \\ \mathcal{R} &= \{(\mathbf{x}_i, \mathbf{x}_j, \mathbf{x}_l) : (\mathbf{x}_i, \mathbf{x}_j) \in \mathcal{S}, y_i \neq y_l\}. \end{aligned}$$

\mathbf{x}_j is termed the target neighbor of \mathbf{x}_i and \mathbf{x}_l is termed the impostor. d_E^2 and d_M^2 denote the squared Euclidean and Mahalanobis distances, respectively; $\mathbf{M} \in \mathbb{S}_+^p$, where \mathbb{S}_+^p is the cone of $p \times p$ real-valued PSD matrices. $\mathbf{M}^2 = \mathbf{M}\mathbf{M}$. $|\mathcal{A}|$ denotes the cardinality of a set \mathcal{A} . $\mathbb{1}_{\{\cdot\}}$ denotes the indicator function. $[a]_+ = \max(a, 0)$ for $a \in \mathbb{R}$.

2 Proposed approach

In this section, we first derive an explicit formula for the support point and provide the rationale behind the advocated perturbation loss, followed by its optimization problem. We then extend the method for high-dimensional data. Lastly, we discuss the benefit of our method to the generalization ability of the learned metric. Main concepts are illustrated in Fig. 2 and listed in Table 5 of Appendix A.

2.1 Support point and perturbation loss

As mentioned in the introduction, a learned distance metric may be sensitive to perturbation in the sense that a small change of the instance could alter its nearest neighbor in the learned feature space, from an instance of the same class to one of a different class, and consequently, increasing the risk of misclassification from k NN. A perturbed point, that causes a change in the nearest neighbors and thus prediction, is termed an *adversarial example* [34]; if the adversarial examples of an instance are all far away from the instance itself, a high degree of robustness is expected. Based on this reasoning, we will construct a loss function to penalize the small distance between a training instance \mathbf{x}_i and its closest adversarial example (i.e. support point), and therefore, allowing \mathbf{x}_i to retain prediction correctness even when perturbed to a larger extent.

We start by building a geometric insight into the support point: for any instance \mathbf{x}_i associated with the triplet constraint $(\mathbf{x}_i, \mathbf{x}_j, \mathbf{x}_l)$, the support point $\mathbf{x}_{i,\min}$ is the closest point to \mathbf{x}_i in the instance space that lies on the decision boundary formed by \mathbf{x}_j and \mathbf{x}_l in the feature space. Note that closeness is defined in the instance space and will be calculated using the Euclidean distance since we target at changes on the original feature of an instance; and that the decision boundary is found in the feature space since k NNs are identified by using the Mahalanobis distance. Mathematically, we can formulate the support point $\mathbf{x}_{i,\min}$ as follows:

$$\mathbf{x}_{i,\min} = \arg \min_{\mathbf{x}'_i \in \mathbb{R}^p} (\mathbf{x}'_i - \mathbf{x}_i)^T \mathbf{A}_0 (\mathbf{x}'_i - \mathbf{x}_i) \quad \text{s.t.} \quad (\mathbf{L}\mathbf{x}'_i - \frac{\mathbf{L}\mathbf{x}_j + \mathbf{L}\mathbf{x}_l}{2})^T (\mathbf{L}\mathbf{x}_l - \mathbf{L}\mathbf{x}_j) = 0. \quad (1)$$

With a pre-given positive definite matrix \mathbf{A}_0 , the objective function of Eq. 1 defines an arbitrarily oriented hyperellipsoid, representing any heterogeneous and correlated perturbation. Without prior knowledge on the perturbation, we simplify \mathbf{A}_0 as the identity matrix. In this case, the objective function defines a hypersphere, representing perturbation of equal magnitude in all directions. It can also be interpreted as minimizing the Euclidean distance from the training instance \mathbf{x}_i . For clarity, we always refer the certified neighborhood as the largest hypersphere in this paper; the hyperellipsoid case is discussed in Appendix B. The constraint defines the decision boundary, which is the perpendicular bisector of points $\mathbf{L}\mathbf{x}_j$ and $\mathbf{L}\mathbf{x}_l$.

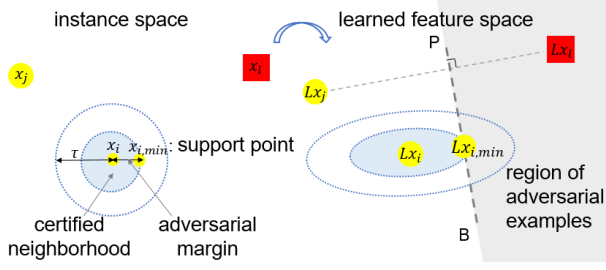


Figure 2: Explanation of main concepts: Given a triplet constraint $(\mathbf{x}_i, \mathbf{x}_j, \mathbf{x}_l)$, the decision boundary for \mathbf{x}_i is the perpendicular bisector of $L\mathbf{x}_j$ and $L\mathbf{x}_l$, i.e. line PB . Points on the right-hand side of PB are adversarial examples. The support point $\mathbf{x}_{i,\min}$ is defined as the nearest adversarial example in the instance space. The Euclidean distance between \mathbf{x}_i and $\mathbf{x}_{i,\min}$ is called adversarial margin; it will be enlarged to τ by penalizing the perturbation loss.

In other words, it is a hyperplane that is perpendicular to the line joining points $L\mathbf{x}_j$ and $L\mathbf{x}_l$ and passes their midpoint $\frac{L\mathbf{x}_j + L\mathbf{x}_l}{2}$; all points on the hyperplane are equidistant from $L\mathbf{x}_j$ and $L\mathbf{x}_l$.

Since Eq. 1 minimizes a convex quadratic function with an equality constraint, we can find an explicit formula for the support point $\mathbf{x}_{i,\min}$ by using the method of Lagrangian multipliers; please see Appendix B for detailed derivation:

$$\mathbf{x}_{i,\min} = \mathbf{x}_i + \frac{(\frac{\mathbf{x}_j + \mathbf{x}_l}{2} - \mathbf{x}_i)^T M(\mathbf{x}_l - \mathbf{x}_j)}{(\mathbf{x}_l - \mathbf{x}_j)^T M^2(\mathbf{x}_l - \mathbf{x}_j)} M(\mathbf{x}_l - \mathbf{x}_j) \quad (2)$$

With a closed-form solution of $\mathbf{x}_{i,\min}$, we can now calculate the squared Euclidean distance between \mathbf{x}_i and $\mathbf{x}_{i,\min}$:

$$d_E^2(\mathbf{x}_i, \mathbf{x}_{i,\min}) = \frac{(d_M^2(\mathbf{x}_i, \mathbf{x}_l) - d_M^2(\mathbf{x}_i, \mathbf{x}_j))^2}{4d_{M^2}^2(\mathbf{x}_j, \mathbf{x}_l)} \quad (3)$$

For clarity, we will call $d_E(\mathbf{x}_i, \mathbf{x}_{i,\min})$ the *adversarial margin*, in contrast to the distance margin as in LMNN. It defines the radius of the certified neighborhood.

To improve robustness of distance metric, we design a perturbation loss to encourage an expansion of certified neighborhood. Two situations need to be distinguished here. Firstly, when the nearest neighbor of \mathbf{x}_i is an instance from the same class, we will penalize a small adversarial margin by using the hinge loss $[\tau^2 - d_E^2(\mathbf{x}_i, \mathbf{x}_{i,\min})]_+$. The reasons are that (a) the adversarial margin is generally smaller for hard instances that are close to the class boundary in contrast to those locating far away and (b) it is these hard instances that are more vulnerable to perturbation and demand an improvement in their robustness. Therefore, we introduce τ for directing attention to hard instances and controlling the desired margin. Secondly, in the other situation where the nearest neighbor of \mathbf{x}_i belongs to a different class, metric learning should focus on satisfying the distance requirement specified in the triplet constraint. In this case, we simply assign a large penalty of τ^2 to promote a non-increasing loss function. Integrating these two situations leads to the proposed perturbation loss:

$$J_P = \frac{1}{|\mathcal{R}|} \sum_{\mathcal{R}} \{ [\tau^2 - \tilde{d}_E^2(\mathbf{x}_i, \mathbf{x}_{i,\min})]_+ \mathbb{1}_{\{d_M^2(\mathbf{x}_i, \mathbf{x}_l) > d_M^2(\mathbf{x}_i, \mathbf{x}_j)\}} + \tau^2 \mathbb{1}_{\{d_M^2(\mathbf{x}_i, \mathbf{x}_l) \leq d_M^2(\mathbf{x}_i, \mathbf{x}_j)\}} \}, \quad (4)$$

where $\sum_{\mathcal{R}}$ is an abbreviation for $\sum_{(\mathbf{x}_i, \mathbf{x}_j, \mathbf{x}_l) \in \mathcal{R}}$. To prevent the denominator of Eq. 3 from being zero, which may happen when different-class instances \mathbf{x}_j and \mathbf{x}_l are close to each other, we add a small constant ϵ ($\epsilon=1e-10$) to the denominator; that is, $\tilde{d}_E^2(\mathbf{x}_i, \mathbf{x}_{i,\min}) = \frac{(d_M^2(\mathbf{x}_i, \mathbf{x}_l) - d_M^2(\mathbf{x}_i, \mathbf{x}_j))^2}{4(d_{M^2}^2(\mathbf{x}_j, \mathbf{x}_l) + \epsilon)}$.

2.2 Metric learning with certified robustness

As support points are derived from triplet constraints, it would be natural and straightforward to embed the proposed perturbation loss into a metric learning method that is also based on triplet constraints. LMNN is thus adopted as an example for its wide use and effective classification performance.

The objective function of the proposed LMNN with certified robustness (LMNN-CR) is as follows:

$$\begin{aligned} \min_{M \in \mathcal{S}_+^p} J &= J_{\text{LMNN}} + \lambda J_P, \\ J_{\text{LMNN}} &= (1 - \mu) \frac{1}{|\mathcal{S}|} \sum_{\mathcal{S}} d_M^2(\mathbf{x}_i, \mathbf{x}_j) + \mu \frac{1}{|\mathcal{R}|} \sum_{\mathcal{R}} [1 + d_M^2(\mathbf{x}_i, \mathbf{x}_j) - d_M^2(\mathbf{x}_i, \mathbf{x}_l)]_+, \end{aligned} \quad (5)$$

where $\sum_{\mathcal{S}}$ stands for $\sum_{(\mathbf{x}_i, \mathbf{x}_j) \in \mathcal{S}}$. The weight parameter $\lambda > 0$ controls the importance of perturbation loss ($J_{\mathcal{P}}$) relative to the loss function of LMNN (J_{LMNN}). $\mu \in (0, 1)$ balances the impacts between pulling together target neighbors and pushing away impostors.

We adopt the projected gradient descent algorithm to solve the optimization problem (Eq. 5). The gradient of $J_{\mathcal{P}}$ and J_{LMNN} are given as follows:

$$\begin{aligned} \frac{\partial J_{\mathcal{P}}}{\partial \mathbf{M}} &= \frac{1}{|\mathcal{R}|} \sum_{\mathcal{R}} \alpha_{ijl} \left\{ \frac{d_{\mathbf{M}}^2(\mathbf{x}_i, \mathbf{x}_l) - d_{\mathbf{M}}^2(\mathbf{x}_i, \mathbf{x}_j)}{2(d_{\mathbf{M}^2}^2(\mathbf{x}_j, \mathbf{x}_l) + \epsilon)} (\mathbf{X}_{ij} - \mathbf{X}_{il}) + \frac{(d_{\mathbf{M}}^2(\mathbf{x}_i, \mathbf{x}_l) - d_{\mathbf{M}}^2(\mathbf{x}_i, \mathbf{x}_j))^2}{4(d_{\mathbf{M}^2}^2(\mathbf{x}_j, \mathbf{x}_l) + \epsilon)^2} (\mathbf{M}\mathbf{X}_{jl} + \mathbf{X}_{jl}\mathbf{M}) \right\}, \\ \frac{\partial J_{\text{LMNN}}}{\partial \mathbf{M}} &= \frac{1 - \mu}{|\mathcal{S}|} \sum_{\mathcal{S}} \mathbf{X}_{ij} + \frac{\mu}{|\mathcal{R}|} \sum_{\mathcal{R}} \beta_{ijl} (\mathbf{X}_{ij} - \mathbf{X}_{il}), \end{aligned}$$

where $\alpha_{ijl} = \mathbb{1}_{\{d_{\mathbf{M}}^2(\mathbf{x}_i, \mathbf{x}_l) > d_{\mathbf{M}}^2(\mathbf{x}_i, \mathbf{x}_j), \tilde{d}_{\mathbf{E}}(\mathbf{x}_i, \mathbf{x}_{i, \min}) \leq \tau\}}$, $\beta_{ijl} = \mathbb{1}_{\{1 + d_{\mathbf{M}}^2(\mathbf{x}_i, \mathbf{x}_j) - d_{\mathbf{M}}^2(\mathbf{x}_i, \mathbf{x}_l) \geq 0\}}$; $\mathbf{X}_{ij} = (\mathbf{x}_i - \mathbf{x}_j)(\mathbf{x}_i - \mathbf{x}_j)^T$ and $\mathbf{X}_{il}, \mathbf{X}_{jl}$ are defined similarly. The gradient of $J_{\mathcal{P}}$ is a sum of two descent directions. The first direction $\mathbf{X}_{ij} - \mathbf{X}_{il}$ agrees with LMNN, indicating that our method updates the metric toward better discrimination in a weighted manner. The second direction $\mathbf{M}\mathbf{X}_{jl} + \mathbf{X}_{jl}\mathbf{M}$ controls the scale of \mathbf{M} ; the metric will descend at a faster pace in the direction of a larger correlation between \mathbf{M} and \mathbf{X}_{jl} . This suggests our method functions as a data-dependent regularization. Let \mathbf{M}^t denote the Mahalanobis matrix learned at the t th iteration. The distance matrix will be updated as

$$\mathbf{M}^{t+1} = \mathbf{M}^t - \gamma \left(\frac{\partial J_{\text{LMNN}}}{\partial \mathbf{M}^t} + \lambda \frac{\partial J_{\mathcal{P}}}{\partial \mathbf{M}^t} \right),$$

where γ denotes the learning rate. To guarantee the PSD property, we factorize \mathbf{M}^{t+1} as $\mathbf{V}\mathbf{\Lambda}\mathbf{V}^T$ via eigendecomposition and truncate all negative eigenvalues to zero, i.e. $\mathbf{M}^{t+1} = \mathbf{V} \max(\mathbf{\Lambda}, 0) \mathbf{V}^T$.

The proposed perturbation loss is a generic approach to improving robustness to perturbation. In Appendix C, we give another example which incorporates the perturbation loss into the recent triplet-based method SCML [31]; the new method is termed SCML with certified robustness (SCML-CR).

2.3 Extension to high-dimensional data

As PCA is often applied to pre-process high-dimensional data prior to metric learning, we propose an extension so that the distance metric learned in the low-dimensional PCA subspace could still achieve certified robustness against perturbation in the original high-dimensional instance space. Defining perturbation loss in conjunction with PCA is realizable as our derivation builds on the linear transformation induced by the distance metric and PCA also performs a linear transformation to map data onto a lower dimension subspace. Let $\mathbf{D} \in \mathbb{R}^{d \times p}$ denote the linear transformation matrix obtained from PCA; p is the original feature dimension and d is the reduced feature dimension. Following same principle as before, the support point $\mathbf{x}_{i, \min}^{\text{PCA}}$ should be the closest point to \mathbf{x}_i in the original high-dimensional instance space and lie on the perpendicular bisector of points $\mathbf{L}\mathbf{D}\mathbf{x}_j$ and $\mathbf{L}\mathbf{D}\mathbf{x}_l$, i.e. after first mapping the data to a low-dimensional subspace by \mathbf{D} and then mapping it to a feature space by \mathbf{L} . The mathematical formulation is as follows:

$$\mathbf{x}_{i, \min}^{\text{PCA}} = \arg \min_{\mathbf{x}'_i} (\mathbf{x}_i - \mathbf{x}'_i)^T (\mathbf{x}_i - \mathbf{x}'_i) \quad \text{s.t.} \quad (\mathbf{L}\mathbf{D}\mathbf{x}'_i - \frac{\mathbf{L}\mathbf{D}\mathbf{x}_j + \mathbf{L}\mathbf{D}\mathbf{x}_l}{2})^T (\mathbf{L}\mathbf{D}\mathbf{x}_l - \mathbf{L}\mathbf{D}\mathbf{x}_j) = 0 \quad (6)$$

As shown in Appendix B.1, $\mathbf{x}_{i, \min}^{\text{PCA}}$ again has a closed-form solution and equations on the adversarial margin and perturbation loss can be extended accordingly.

2.4 Generalization benefit

From the perspective of algorithmic robustness [43], enlarging the adversarial margin could potentially improve the generalization ability of triplet-based metric learning methods. The following generalization bound, i.e. the gap between the generalization error \mathcal{L} and the empirical error ℓ_{emp} , follows from the pseudo-robust theorem of [2]. Preliminaries and derivations are given in Appendix D.

Theorem 1. Let \mathbf{M}^* be the optimal solution to Eq. 5. Then for any $\delta > 0$, with probability at least $1 - \delta$ we have:

$$|\mathcal{L}(\mathbf{M}^*) - \ell_{\text{emp}}(\mathbf{M}^*)| \leq \frac{\hat{n}(t_{\mathbf{s}})}{n^3} + B \left(\frac{n^3 - \hat{n}(t_{\mathbf{s}})}{n^3} + 3\sqrt{\frac{2K \ln 2 + 2 \ln 1/\delta}{n}} \right), \quad (7)$$

Table 1: Classification accuracy (mean±standard deviation) of 3NN on clean datasets.

Dataset	LMNN-based						SCML-based	
	AML	LMNN	LDD	CAP	DRIFT	LMNN-CR	SCML	SCML-CR
Australian	83.25 ±2.59	83.70±2.43	84.18±2.37	83.97±2.45	84.47±2.02	84.47±1.63	84.76±2.08	84.42±2.18
Breast cancer	97.10 ±1.21	97.12±1.25	96.95±1.51	97.00±1.08	96.98±1.16	97.02±1.30	97.00±1.09	97.07±1.24
Fourclass	75.12 ±2.35	75.10±2.31	75.15±2.32	75.02±2.48	75.08±2.34	<u>75.12±2.35</u>	75.10±2.27	75.12±2.35
Haberman	72.58 ±4.00	72.19±3.89	<u>72.42±3.95</u>	71.52±3.54	72.02±3.94	72.64±4.29	72.75±3.79	72.36±4.38
Iris	87.00 ±5.41	87.11±5.08	87.67±4.70	86.67±5.49	85.89±4.46	87.33±4.73	86.89±6.40	87.44±5.31
Segment	95.21 ±0.72	95.31±0.89	95.58±0.81	95.51±0.70	95.75±0.65	<u>95.64±0.83</u>	92.61±6.65	93.95±1.47
Sonar	84.13 ±4.86	86.67±4.10	<u>87.22±3.90</u>	<u>87.22±4.38</u>	86.19±4.43	87.78±3.53	82.38±4.15	84.13±4.61
Voting	95.34 ±1.64	95.80±1.78	95.80±1.41	<u>95.92±1.45</u>	95.31±1.32	96.15±1.56	95.84±1.58	96.26±1.28
WDBC	96.93 ±1.39	<u>96.99±1.30</u>	96.96±1.43	<u>96.99±1.51</u>	96.70±1.16	97.13±1.33	97.25±1.30	97.25±1.52
Wine	97.13 ±1.75	<u>97.31±1.94</u>	96.67±1.76	<u>96.85±2.26</u>	97.69±1.79	97.69±1.89	97.69±1.79	97.22±2.04
# outperform	-	9	8	10	9	-	7	-

For methods with LMNN as the backbone, the best ones are shown in bold and the second best ones are underlined; for methods with SCML as the backbone, the best ones are shown in bold. ‘# outperform’ counts the number of datasets where LMNN-CR (SCML-CR, resp.) outperforms or performs equally well with LMNN-based (SCML, resp.) methods.

where $\hat{n}(t_s)$ denotes the number of triplets whose adversarial margins are larger than τ , B is a constant denoting the upper bound of the loss function (i.e. Eq. 5), and $K = |\mathcal{Y}|(1 + \frac{2}{\tau})^p$.

Enlarging the desired adversarial margin τ will reduce the value of K and $\hat{n}(t_s)$ in Eq. 9. On the one hand, K decreases with τ at a polynomial rate of the input dimensionality p and hence the upper bound of generalization gap reduces at a rate of $p^{1/2}$. On the other hand, the reduction in $\hat{n}(t_s)$ increases the upper bound. However, $\hat{n}(t_s)$ remains relatively stable when τ increases as long as most instances in the dataset do not have a small margin in the original instance space. Therefore, for this type of dataset, we expect an improvement in the generalization ability of the learned distance metric from enlarging the adversarial margin.

3 Experiments

In this section, we evaluate the generalization performance and robustness of the proposed method on 12 benchmark datasets (10 low/medium-dimensional and two high-dimensional), followed by a comparison of computational cost. In Appendix E.3, we present experiments on three synthetic datasets to illustrate the difference in the learning behavior between LMNN and the proposed method.

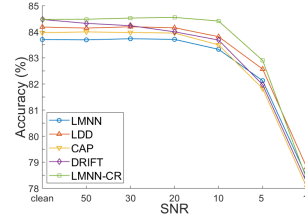
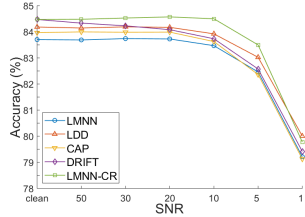
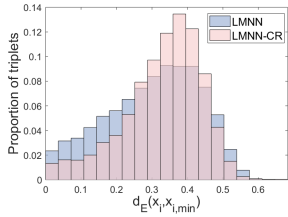
3.1 Experiments on UCI data

3.1.1 Data description and experimental setting

We evaluate the proposed LMNN-CR and SCML-CR on 10 UCI datasets [10]. All datasets are pre-processed with mean-centering and standardization, followed by L_2 normalization to unit length. We use 70-30% training-test partitions and report the performance over 20 rounds.

The proposed methods are compared with two types of methods. First, we consider different regularizers on M . Specifically, we replace the regularizer in LMNN from $\sum_{\mathcal{S}} d_M^2(\mathbf{x}_i, \mathbf{x}_j)$ to the log-determinant divergence (LDD) [7], which encourages learning a metric toward the identity matrix, and to the capped trace norm (CAP) [15], which encourages a low-rank matrix. Second, we compare with the method DRIFT [48], which models the perturbation distribution explicitly. We also report the performance of adversarial metric learning (AML) [6]. However, it is not directly comparable to our method as it learns from pairwise constraints. In all experiments, triplet constraints are generated from 3 target neighbors and 10 nearest impostors, calculated under the Euclidean distance.

Hyperparameters of our methods are tuned via random search [4]. We randomly sample 50 sets of values from the following ranges: $\mu \in U(0.1, 0.9)$, $\tau \in U(0, P_{90\%}\{d_E(\mathbf{x}_i, \mathbf{x}_{i,\min})\})$, $\lambda \in U(0, 4/\tau^2)$. $U(a, b)$ denotes the uniform distribution. $P_{k\%}\{d_E(\mathbf{x}_i, \mathbf{x}_{i,\min})\}$ denotes the k th percentile of $d_E(\mathbf{x}_i, \mathbf{x}_{i,\min})$, where $\mathbf{x}_{i,\min}$ is calculated with respect to the Euclidean distance. Information about the datasets, optimization details of the proposed and other methods, and evaluation of hyperparameter sensitivity are given in Appendices E.1, E.2, E.5, respectively.



(a) Histogram of adversarial margins after metric learning from LMNN and LMNN-CR.

(b) Performance of LMNN-based methods under different levels of spherical Gaussian noise.

(c) Performance of LMNN-based methods under different levels of Gaussian noise.

Table 2: Classification accuracy of 3NN on datasets contaminated with Gaussian noise (SNR=5 dB).

Dataset	AML	LMNN-based					SCML-based	
		LMNN	LDD	CAP	DRIFT	LMNN-CR	SCML	SCML-CR
Australian	82.26 ± 1.62	82.13 ± 1.52	82.57 ± 1.55	81.82 ± 1.52	81.97 ± 1.53	82.90 ± 1.53	82.59 ± 1.70	82.84 ± 1.64
Breast cancer	96.70 ± 1.01	96.24 ± 1.06	96.66 ± 1.07	96.27 ± 1.03	96.61 ± 0.97	96.69 ± 1.07	96.34 ± 1.03	96.63 ± 1.03
Fourclass	69.00 ± 1.06	67.74 ± 1.25	68.84 ± 1.14	67.84 ± 1.19	69.13 ± 1.02	69.04 ± 1.11	68.22 ± 1.10	68.96 ± 1.11
Haberman	70.21 ± 1.84	70.21 ± 1.84	70.25 ± 1.82	69.39 ± 2.06	69.31 ± 2.50	70.25 ± 1.90	69.98 ± 1.64	70.24 ± 1.85
Iris	79.07 ± 3.25	78.75 ± 2.96	79.04 ± 3.17	77.90 ± 3.31	78.57 ± 3.09	79.20 ± 3.08	78.32 ± 3.60	79.18 ± 3.13
Segment	85.87 ± 0.70	79.03 ± 3.37	83.49 ± 1.17	82.77 ± 2.49	83.88 ± 1.33	82.13 ± 2.70	61.28 ± 9.78	62.86 ± 8.76
Sonar	83.50 ± 3.38	83.54 ± 4.30	86.18 ± 2.93	85.44 ± 2.79	84.65 ± 3.30	84.99 ± 3.13	76.91 ± 4.32	79.49 ± 3.80
Voting	94.10 ± 1.07	94.01 ± 1.00	94.24 ± 1.13	94.37 ± 1.17	93.94 ± 1.12	94.64 ± 1.21	93.99 ± 1.15	94.65 ± 1.09
WDBC	96.47 ± 1.12	92.01 ± 1.65	96.30 ± 0.94	96.14 ± 1.11	96.02 ± 0.88	96.07 ± 0.89	95.75 ± 1.29	96.22 ± 1.14
Wine	95.03 ± 1.14	93.27 ± 1.62	93.97 ± 1.38	93.87 ± 1.49	94.55 ± 1.15	94.44 ± 1.21	93.92 ± 1.55	94.52 ± 1.33
# outperform	-	10	6	7	7	-	10	-

3.1.2 Evaluation on classification performance

Table 1 reports classification accuracy of 3NN. LMNN-CR outperforms LMNN on 9 out of 10 datasets. Among the methods with LMNN as the backbone, our method achieves the highest accuracy on 6 datasets and second highest accuracy on the remaining 4 datasets. SCML-CL outperforms or performs equally well with SCML on 7 datasets. These experimental results demonstrate the benefit of perturbation loss to generalization of the learned distance metric.

3.1.3 Investigation into robustness

We start with an in-depth study on the dataset Australian to investigate the relationship between the perturbation loss, adversarial margin and robustness against instance perturbation. First, we compare the adversarial margins obtained from LMNN and LMNN-CR. Instances with near-zero adversarial margins are incapable of defending perturbation. From Fig. 3a, we see that nearly half of these vulnerable instances have a larger adversarial margin after learning with the proposed loss. Next, we evaluate robustness by adding two types of zero-mean Gaussian noise to test data, namely *spherical Gaussian* with a diagonal covariance matrix and equal variances and *Gaussian* with unequal variances. The noise intensity is controlled via the signal-to-noise ratio (SNR). In addition, test data is augmented to the sample size of 10,000. Fig. 3b plots the classification accuracy of LMNN-based methods under different levels of spherical Gaussian noise. When the noise intensity is low, the performance of LMNN and LMNN-CR remain stable. When the noise intensity increases to the SNR of 10 dB or 5 dB, the performances of both method degrade. Owing to the enlarged adversarial margin, the influence on LMNN-CR is slightly smaller than that on LMNN. When the SNR equals 1 dB, the performance gain from using LMNN-CR becomes smaller. This result is reasonable as the desired margin τ is selected according to the criterion of classification accuracy and hence may be too small to withstand a high level of noise. LMNN-CR surpasses all other LMNN-based methods until the noise intensity is very large. Fig. 3c plots the accuracy under the Gaussian noise. The degradation of all methods is more pronounced in this case, but the pattern remains similar.

We now turn to test robustness on all data sets. Gaussian noise of 5 dB is added to the test data. Table 2 shows that LMNN-CR and SCML-CR improve the robustness of the corresponding baselines on all datasets, which clearly demonstrates the benefit of perturbation loss to improving robustness.

Table 3: Generalization and robustness of DML methods on high-dimensional datasets.

Method	Isolet						MNIST					
	Clean	SG-20 (0.081)	SG-5 (0.423)	G-20 (0.059)	G-5 (0.318)	Adv. margin	Clean	SG-20 (0.054)	SG-5 (0.294)	G-20 (0.065)	G-5 (0.348)	Adv. margin
LMNN	90.1 ±4.5	90.1 ±4.1	86.0 ±3.5	90.2 ±4.0	87.8 ±3.9	0.110	90.6	90.0	88.4	90.1	88.4	0.153
LMNN-CR	91.1 ±3.7	91.0 ±3.8	87.9 ±3.3	91.1 ±3.7	89.4 ±3.8	0.125	91.2	91.4	90.8	91.5	90.4	0.223
CAP	91.1 ±3.7	91.1 ±3.9	89.0 ±4.0	91.1 ±3.7	89.9 ±3.9	0.151	91.7	91.8	91.4	91.8	90.7	0.222
CAP-CR	91.6 ±4.0	91.5 ±3.9	89.9 ±3.7	91.5 ±3.9	90.7 ±3.7	0.156	92.0	91.9	90.9	92.0	90.7	0.226
SCML	90.7 ±4.1	90.3 ±4.2	86.5 ±4.2	90.5 ±4.1	88.5 ±3.7	0.068	89.0	88.8	87.4	88.9	86.5	0.122
SCML-CR	90.8 ±4.2	90.7 ±4.1	86.5 ±3.7	90.8 ±4.2	88.4 ±4.1	0.082	89.2	89.2	88.5	89.4	88.1	0.143

Columns 3-6 and 9-12 report methods' robustness against spherical Gaussian noise and Gaussian noise with SNR of 20 dB and 5 dB. Values in brackets are the average perturbation size, calculated as the mean value of the L_2 norm of noises ($\|\Delta \mathbf{x}_i\|_2$).

Moreover, LMNN-CR is superior to the robust metric learning methods CAP and DRIFT on 7 datasets. The method LDD is also quite robust to perturbation. However, this should not be surprising as it encourages learning a metric close to the Euclidean distance, and the Euclidean distance is less sensitive to perturbation than the discriminative Mahalanobis distance. The performance under spherical Gaussian noise is similar to the Gaussian noise, as shown in Appendix E.4.

3.2 Experiments on high-dimensional data

We verify the efficacy of the extended LMNN-CR proposed in Sec. 2.3 on the following datasets:

1. MNIST-2k [5]: The dataset includes the first 2,000 training images and first 2,000 test images of the MNIST database. We apply PCA to reduce the feature dimension from 784 to 141, accounting for 95% of total variance. All methods are evaluated once on the pre-given training/test partition.
2. Isolet [10]: This spoken letter database includes 7,797 instances, grouped into four training sets and one test set. Applying PCA reduces the feature dimension from 617 to 170. All methods are trained four times, one time on each training set, and evaluated on the pre-given test set.

In addition, we introduce CAP-CR, which comprises the triplet loss of LMNN, the proposed perturbation loss, and the low-rank regularizer of CAP. For a fair comparison, CAP-CR uses the same rank and regularization weight as CAP; τ, λ are tuned from 10 randomly sampled sets of values.

Table 3 compares the generalization and robustness performance of LMNN, CAP, SCML and our method; the accuracy of other methods are inferior to LMNN-CR and are reported in Appendix E.4. First, on both datasets, our method achieves higher clean accuracy than the baseline methods, validating its effectiveness in enhancing the generalization ability of the learned distance metric. Second, when the average adversarial margin is larger than the average perturbation size (SNR=20 dB), our method maintains its superiority, demonstrating that adversarial margin is indeed a contributing factor in achieving certified robustness. When the margin is smaller than the perturbation size, our method could still improve the accuracy for LMNN on both datasets, for CAP on Isolet, and for SCML on MNIST. Third, CAP-CR obtains higher accuracy on both clean and noise-contaminated data than LMNN-CR, suggesting that regularization and perturbation loss impose different requirements on \mathbf{M} and combining them has the potential for learning a more effective distance metric.

3.3 Computational cost

We now analyze the computational complexity of LMNN-CR. According to Eq. 6, our method requires additional calculations on $d_{M^2}^2(\mathbf{x}_j, \mathbf{x}_l)$ and $\mathbf{M}\mathbf{X}_{jl}$. Given $|\mathcal{R}|$ triplets, the computational complexity of $d_{M^2}^2(\mathbf{x}_j, \mathbf{x}_l)$ is $O(p^2 + |\mathcal{R}|p)$; given n training instances, the computational complexity of $\mathbf{M}\mathbf{X}_{jl}$ is $O(np^2)$. The total complexity of our method is $O(p^3 + np^2 + |\mathcal{R}|p)$, same as that of LMNN.

Table 4: Average training time (in seconds) of LMNN-based methods.

	LMNN	LDD	CAP	DRIFT	LMNN-CR
Australian	13.44	0.83	3.07	1.00	2.15
Segment	27.48	10.45	11.47	5.12	19.54
Sonar	4.93	4.08	4.65	0.92	6.75
WDBC	9.38	2.94	5.22	5.12	8.17
Isolet	339.57	207.69	176.50	N/A	190.55
MNIST	369.55	68.98	180.68	37.51	391.04

Table 4 compares the running time of LMNN-based methods on four UCI datasets that are large in sample size or in dimensionality and two high-dimensional datasets. The computational cost of our method is comparable to LMNN.

4 Conclusion

In this paper, we demonstrate that robustness and generalization of distance metrics can be enhanced by enforcing a larger margin in the instance space. By taking advantage of the linear transformation induced by the Mahalanobis distance, we obtain an explicit formula for the support points and push them away from training instances through penalizing the perturbation loss. Extensive experiments verify that our method effectively enlarges the adversarial margin, achieves certified robustness, and sustains classification excellence. Future work include jointly learning the perturbation distribution and distance metric and extending the idea to nonlinear metric learning methods.

References

- [1] S. An, M. Hayat, S. H. Khan, M. Bennamoun, F. Boussaid, and F. Sohel. Contractive rectifier networks for nonlinear maximum margin classification. In *IEEE International Conference on Computer Vision*, pages 2515–2523, 2015.
- [2] A. Bellet and A. Habrard. Robustness and generalization for metric learning. *Neurocomputing*, 151:259–267, 2015.
- [3] A. Bellet, A. Habrard, and M. Sebban. Metric learning. *Synthesis Lectures on Artificial Intelligence and Machine Learning*, 9(1):1–151, 2015.
- [4] J. Bergstra and Y. Bengio. Random search for hyper-parameter optimization. *Journal of Machine Learning Research*, 13(Feb):281–305, 2012.
- [5] D. Cai, X. He, J. Han, and T. S. Huang. Graph regularized nonnegative matrix factorization for data representation. *IEEE Transactions on Pattern Analysis and Machine Intelligence*, 33(8):1548–1560, 2010. Data: <http://www.cad.zju.edu.cn/home/dengcai/Data/MLData.html>.
- [6] S. Chen, C. Gong, J. Yang, X. Li, Y. Wei, and J. Li. Adversarial metric learning. In *International Joint Conference on Artificial Intelligence*, pages 2021–2027. AAAI Press, 2018.
- [7] J. V. Davis, B. Kulis, P. Jain, S. Sra, and I. S. Dhillon. Information-theoretic metric learning. In *International Conference on Machine Learning*, pages 209–216. ACM, 2007.
- [8] G. W. Ding, Y. Sharma, K. Y. C. Lui, and R. Huang. MMA training: Direct input space margin maximization through adversarial training. In *International Conference on Learning Representations*, 2020.
- [9] M. Dong, Y. Wang, X. Yang, and J.-H. Xue. Learning local metrics and influential regions for classification. *IEEE Transactions on Pattern Analysis and Machine Intelligence*, 42(6):1522–1529, 2020.
- [10] D. Dua and C. Graff. UCI machine learning repository, 2017.
- [11] Y. Duan, W. Zheng, X. Lin, J. Lu, and J. Zhou. Deep adversarial metric learning. In *IEEE Conference on Computer Vision and Pattern Recognition*, pages 2780–2789, 2018.
- [12] G. Elsayed, D. Krishnan, H. Mobahi, K. Regan, and S. Bengio. Large margin deep networks for classification. In *Advances in Neural Information Processing Systems*, pages 842–852, 2018.
- [13] L. Gautheron, A. Habrard, E. Morvant, and M. Sebban. Metric learning from imbalanced data with generalization guarantees. *Pattern Recognition Letters*, 133:298–304, 2020.
- [14] J. Hu, J. Lu, and Y.-P. Tan. Sharable and individual multi-view metric learning. *IEEE Transactions on Pattern Analysis and Machine Intelligence*, 40(9):2281–2288, 2017.

- [15] Z. Huo, F. Nie, and H. Huang. Robust and effective metric learning using capped trace norm: Metric learning via capped trace norm. In *ACM SIGKDD International Conference on Knowledge Discovery and Data Mining*, pages 1605–1614. ACM, 2016.
- [16] R. Jin, S. Wang, and Y. Zhou. Regularized distance metric learning: Theory and algorithm. In *Advances in Neural Information Processing Systems*, pages 862–870, 2009.
- [17] M. Koestinger, M. Hirzer, P. Wohlhart, P. M. Roth, and H. Bischof. Large scale metric learning from equivalence constraints. In *IEEE Conference on Computer vision and Pattern Recognition*, pages 2288–2295. IEEE, 2012.
- [18] B. Kulis et al. Metric learning: A survey. *Foundations and Trends® in Machine Learning*, 5(4):287–364, 2013.
- [19] J. T. Kwok and I. W. Tsang. Learning with idealized kernels. In *International Conference on Machine Learning*, pages 400–407, 2003.
- [20] M. T. Law, N. Thome, and M. Cord. Quadruplet-wise image similarity learning. In *IEEE International Conference on Computer Vision*, pages 249–256, 2013.
- [21] M. T. Law, N. Thome, and M. Cord. Fantope regularization in metric learning. In *IEEE Conference on Computer Vision and Pattern Recognition*, pages 1051–1058, 2014.
- [22] X. Li, L. Yu, C.-W. Fu, M. Fang, and P.-A. Heng. Revisiting metric learning for few-shot image classification. *Neurocomputing*, 2020.
- [23] D. Lim, G. Lanckriet, and B. McFee. Robust structural metric learning. In *International Conference on Machine Learning*, pages 615–623, 2013.
- [24] H. Liu, Z. Han, Y.-S. Liu, and M. Gu. Fast low-rank metric learning for large-scale and high-dimensional data. In *Advances in Neural Information Processing Systems*, pages 817–827, 2019.
- [25] K. Liu, L. Brand, H. Wang, and F. Nie. Learning robust distance metric with side information via ratio minimization of orthogonally constrained $\ell_{2,1}$ -norm distances. In *International Joint Conference on Artificial Intelligence*, 2019.
- [26] L. Luo and H. Huang. Matrix variate Gaussian mixture distribution steered robust metric learning. In *AAAI Conference on Artificial Intelligence*, 2018.
- [27] B. McFee and G. R. Lanckriet. Metric learning to rank. In *International Conference on Machine Learning*, pages 775–782, 2010.
- [28] K. B. Petersen and M. S. Pedersen. The matrix cookbook, nov 2012. URL <http://www2.imm.dtu.dk/pubdb/p.php/3274>, 2012.
- [29] Q. Qian, J. Tang, H. Li, S. Zhu, and R. Jin. Large-scale distance metric learning with uncertainty. In *IEEE Conference on Computer Vision and Pattern Recognition*, pages 8542–8550, 2018.
- [30] K. Roth, T. Milbich, S. Sinha, P. Gupta, B. Ommer, and J. P. Cohen. Revisiting training strategies and generalization performance in deep metric learning. In *International Conference on Machine Learning*, 2020.
- [31] Y. Shi, A. Bellet, and F. Sha. Sparse compositional metric learning. In *AAAI Conference on Artificial Intelligence*, 2014.
- [32] K. Sohn. Improved deep metric learning with multi-class n-pair loss objective. In *Advances in Neural Information Processing Systems*, pages 1857–1865, 2016.
- [33] K. Song, F. Nie, J. Han, and X. Li. Parameter free large margin nearest neighbor for distance metric learning. In *AAAI Conference on Artificial Intelligence*, 2017.
- [34] C. Szegedy, W. Zaremba, I. Sutskever, J. Bruna, D. Erhan, I. Goodfellow, and R. Fergus. Intriguing properties of neural networks. *arXiv preprint arXiv:1312.6199*, 2013.

- [35] R. Tibshirani. CMU Machine Learning 10-725 Lecture Slides: Proximal Gradient Descent and Acceleration, 2015. URL: <https://www.stat.cmu.edu/~ryantibs/convexopt-S15/lectures/08-prox-grad.pdf>. Last visited on 18/May/2020.
- [36] M. J. Wainwright. *Metric entropy and its uses*, pages 121–158. Cambridge Series in Statistical and Probabilistic Mathematics. Cambridge University Press, 2019.
- [37] H. Wang, F. Nie, and H. Huang. Robust distance metric learning via simultaneous ℓ_1 -norm minimization and maximization. In *International Conference on Machine Learning*, pages 1836–1844, 2014.
- [38] X. Wang, X. Han, W. Huang, D. Dong, and M. R. Scott. Multi-similarity loss with general pair weighting for deep metric learning. In *IEEE Conference on Computer Vision and Pattern Recognition*, pages 5022–5030, 2019.
- [39] K. Q. Weinberger and L. K. Saul. Distance metric learning for large margin nearest neighbor classification. *Journal of Machine Learning Research*, 10(Feb):207–244, 2009.
- [40] S. Xiang, F. Nie, and C. Zhang. Learning a Mahalanobis distance metric for data clustering and classification. *Pattern Recognition*, 41(12):3600–3612, 2008.
- [41] E. P. Xing, M. I. Jordan, S. J. Russell, and A. Y. Ng. Distance metric learning with application to clustering with side-information. In *Advances in Neural Information Processing Systems*, pages 521–528, 2003.
- [42] H. Xiong and X.-w. Chen. Kernel-based distance metric learning for microarray data classification. *BMC Bioinformatics*, 7(1):1–11, 2006.
- [43] H. Xu and S. Mannor. Robustness and generalization. *Machine learning*, 86(3):391–423, 2012.
- [44] J. Xu, L. Luo, C. Deng, and H. Huang. Bilevel distance metric learning for robust image recognition. In *Advances in Neural Information Processing Systems*, pages 4198–4207, 2018.
- [45] Z. Yan, Y. Guo, and C. Zhang. Adversarial margin maximization networks. *IEEE Transactions on Pattern Analysis and Machine Intelligence*, 2019.
- [46] J. Yang, D. She, Y.-K. Lai, and M.-H. Yang. Retrieving and classifying affective images via deep metric learning. In *AAAI Conference on Artificial Intelligence*, 2018.
- [47] L. Yang and R. Jin. Distance metric learning: A comprehensive survey. *Michigan State University*, 2(2):4, 2006.
- [48] H.-J. Ye, D.-C. Zhan, X.-M. Si, and Y. Jiang. Learning Mahalanobis distance metric: considering instance disturbance helps. In *International Joint Conference on Artificial Intelligence*, pages 3315–3321. AAAI Press, 2017.

A Summary of main concepts

Table 5: Terminology list

adversarial example	a perturbed instance; the perturbation changes the label of the instance's nearest neighbor (NN) in the feature space from being the same class to being a different class. In other words, the perturbation forces the NN classifier to produce an incorrect prediction [34].
support point ($\mathbf{x}_{i,\min}$)	the adversarial example that is closest to the training instance in the original instance space
certified neighborhood	the largest hypersphere that a training instance could be perturbed while keeping its NN in the feature space to be an instance of the same class
adversarial margin ($d_E(\mathbf{x}_i, \mathbf{x}_{i,\min})$)	the Euclidean distance between a training instance and its associated support point. It defines the radius of certified neighborhood.

B Derivation of support point, adversarial margin, and gradient of perturbation loss

First, we define the hyperellipsoid via the quadratic form. An arbitrarily oriented hyperellipsoid, centered at $\boldsymbol{\mu} \in \mathbb{R}^p$, is defined by the solutions to the equation

$$\{\mathbf{x} \in \mathbb{R}^p : (\mathbf{x} - \boldsymbol{\mu})^T \mathbf{A}_0 (\mathbf{x} - \boldsymbol{\mu}) = r^2\},$$

where \mathbf{A}_0 is a positive definite matrix. By the Cholesky decomposition, $\mathbf{A}_0 = \mathbf{A}\mathbf{A}^T$. Therefore, finding the support point of \mathbf{x}_i on the hyperellipsoid is equivalent to finding the point \mathbf{x}'_i that defines the smallest hypersphere given by $(\mathbf{A}^T(\mathbf{x}'_i - \mathbf{x}_i))^T(\mathbf{A}^T(\mathbf{x}'_i - \mathbf{x}_i)) = r^2$.

The optimization problem of Eq. 1 is equivalent to the following problem:

$$\begin{aligned} \mathbf{x}_{i,\min} &= \arg \min_{\mathbf{x}'_i \in \mathbb{R}^p} (\mathbf{A}^T(\mathbf{x}'_i - \mathbf{x}_i))^T(\mathbf{A}^T(\mathbf{x}'_i - \mathbf{x}_i)) \\ \text{s.t. } &(\mathbf{L}\mathbf{x}'_i - \frac{\mathbf{L}\mathbf{x}_j + \mathbf{L}\mathbf{x}_l}{2})^T(\mathbf{L}\mathbf{x}_l - \mathbf{L}\mathbf{x}_j) = 0. \end{aligned}$$

Applying the method of Lagrangian multiplier, we transform the above problem to the following Lagrangian function by introducing the Lagrangian multiplier λ and then solve it by setting the first partial derivatives to zero:

$$\begin{aligned} &\min_{\mathbf{x}'_i} (\mathbf{A}^T(\mathbf{x}'_i - \mathbf{x}_i))^T(\mathbf{A}^T(\mathbf{x}'_i - \mathbf{x}_i)) - \lambda(\mathbf{L}\mathbf{x}'_i - \frac{\mathbf{L}\mathbf{x}_j + \mathbf{L}\mathbf{x}_l}{2})^T(\mathbf{L}\mathbf{x}_l - \mathbf{L}\mathbf{x}_j) \\ &\frac{\delta}{\delta \mathbf{x}'_i} : 2\mathbf{A}\mathbf{A}^T(\mathbf{x}'_i - \mathbf{x}_i) - \lambda\mathbf{L}^T\mathbf{L}(\mathbf{x}_l - \mathbf{x}_j) = 0 \\ &\mathbf{x}'_i = \mathbf{x}_i + \frac{\lambda}{2}\mathbf{A}_0^{-1}\mathbf{L}^T\mathbf{L}(\mathbf{x}_l - \mathbf{x}_j) \\ &(\mathbf{L}\mathbf{x}_i + \frac{\lambda}{2}\mathbf{L}\mathbf{A}_0^{-1}\mathbf{L}^T\mathbf{L}(\mathbf{x}_l - \mathbf{x}_j) - \frac{\mathbf{L}\mathbf{x}_j + \mathbf{L}\mathbf{x}_l}{2})^T(\mathbf{L}\mathbf{x}_l - \mathbf{L}\mathbf{x}_j) = 0 \\ &\frac{\lambda}{2} = \frac{(\frac{\mathbf{x}_j + \mathbf{x}_l}{2} - \mathbf{x}_i)^T\mathbf{L}^T\mathbf{L}(\mathbf{x}_l - \mathbf{x}_j)}{(\mathbf{x}_l - \mathbf{x}_j)^T\mathbf{L}^T\mathbf{L}\mathbf{A}_0^{-1}\mathbf{L}^T\mathbf{L}(\mathbf{x}_l - \mathbf{x}_j)} \\ &\mathbf{x}_{i,\min} = \mathbf{x}_i + \frac{(\frac{\mathbf{x}_j + \mathbf{x}_l}{2} - \mathbf{x}_i)^T\mathbf{M}(\mathbf{x}_l - \mathbf{x}_j)}{(\mathbf{x}_l - \mathbf{x}_j)^T\mathbf{M}\mathbf{A}_0^{-1}\mathbf{M}(\mathbf{x}_l - \mathbf{x}_j)}\mathbf{A}_0^{-1}\mathbf{M}(\mathbf{x}_l - \mathbf{x}_j). \end{aligned}$$

The Hessian matrix equals $2\mathbf{A}_0$, which is positive definite, and hence $\mathbf{x}_{i,\min}$ is the minimum point. Replacing $\mathbf{A}_0 = \mathbf{I}$ (identity matrix) gives Eq. 2.

The squared adversarial margin is calculated by first simplifying $\mathbf{x}_{i,\min}$ and then computing r^2 as follows:

$$\begin{aligned}
& \left(\frac{\mathbf{x}_j + \mathbf{x}_l}{2} - \mathbf{x}_i\right)^T \mathbf{M}(\mathbf{x}_l - \mathbf{x}_j) \\
&= \frac{1}{2} \left((\mathbf{x}_j - \mathbf{x}_i) + (\mathbf{x}_l - \mathbf{x}_i) \right)^T \mathbf{M} \left((\mathbf{x}_l - \mathbf{x}_i) - (\mathbf{x}_j - \mathbf{x}_i) \right) \\
&= \frac{1}{2} \left(d_M^2(\mathbf{x}_i, \mathbf{x}_l) - d_M^2(\mathbf{x}_i, \mathbf{x}_j) \right) \\
r^2 &= (\mathbf{x}_i - \mathbf{x}_{i,\min})^T \mathbf{A}_0 (\mathbf{x}_i - \mathbf{x}_{i,\min}) \\
&= \left(\frac{d_M^2(\mathbf{x}_i, \mathbf{x}_l) - d_M^2(\mathbf{x}_i, \mathbf{x}_j)}{2(\mathbf{x}_l - \mathbf{x}_j)^T \mathbf{M} \mathbf{A}_0^{-1} \mathbf{M} (\mathbf{x}_l - \mathbf{x}_j)} \mathbf{A}_0^{-1} \mathbf{L}^T \mathbf{L} (\mathbf{x}_l - \mathbf{x}_j) \right)^T \\
&\quad \mathbf{A}_0 \left(\frac{d_M^2(\mathbf{x}_i, \mathbf{x}_l) - d_M^2(\mathbf{x}_i, \mathbf{x}_j)}{2(\mathbf{x}_l - \mathbf{x}_j)^T \mathbf{M} \mathbf{A}_0^{-1} \mathbf{M} (\mathbf{x}_l - \mathbf{x}_j)} \mathbf{A}_0^{-1} \mathbf{L}^T \mathbf{L} (\mathbf{x}_l - \mathbf{x}_j) \right) \\
&= \frac{(d_M^2(\mathbf{x}_i, \mathbf{x}_l) - d_M^2(\mathbf{x}_i, \mathbf{x}_j))^2}{4 \left((\mathbf{x}_l - \mathbf{x}_j)^T \mathbf{M} \mathbf{A}_0^{-1} \mathbf{M} (\mathbf{x}_l - \mathbf{x}_j) \right)^2} \cdot (\mathbf{x}_l - \mathbf{x}_j)^T \mathbf{L}^T \mathbf{L} \mathbf{A}_0^{-1} \mathbf{A}_0 \mathbf{A}_0^{-1} \mathbf{L}^T \mathbf{L} (\mathbf{x}_l - \mathbf{x}_j) \\
&= \frac{(d_M^2(\mathbf{x}_i, \mathbf{x}_l) - d_M^2(\mathbf{x}_i, \mathbf{x}_j))^2}{4 \left((\mathbf{x}_l - \mathbf{x}_j)^T \mathbf{M} \mathbf{A}_0^{-1} \mathbf{M} (\mathbf{x}_l - \mathbf{x}_j) \right)}.
\end{aligned}$$

Substituting $\mathbf{A}_0 = \mathbf{I}$ gives Eq. 3.

Next, we derive the gradient of $J_{\mathcal{P}}$ with respect to \mathbf{M} . When $d_M^2(\mathbf{x}_i, \mathbf{x}_l) > d_M^2(\mathbf{x}_i, \mathbf{x}_j)$ and $r \geq \tau$ (i.e. $\tilde{d}_{\mathbf{E}}(\mathbf{x}_i, \mathbf{x}_{i,\min}) \geq \tau$ in the hyperspherical case), or $d_M^2(\mathbf{x}_i, \mathbf{x}_l) \leq d_M^2(\mathbf{x}_i, \mathbf{x}_j)$, the gradient equals zero. When $d_M^2(\mathbf{x}_i, \mathbf{x}_l) > d_M^2(\mathbf{x}_i, \mathbf{x}_j)$ and $r < \tau$, the gradient of $J_{\mathcal{P}}$ equals the gradient of $-r^2$ (i.e. $-\tilde{d}_{\mathbf{E}}^2(\mathbf{x}_i, \mathbf{x}_{i,\min})$ in the hyperspherical case), which can be calculated by using the quotient rule and the derivative of trace [28]:

$$\begin{aligned}
& \frac{\partial}{\partial \mathbf{M}} \left(d_M^2(\mathbf{x}_i, \mathbf{x}_l) - d_M^2(\mathbf{x}_i, \mathbf{x}_j) \right)^2 \\
&= 2 \left(d_M^2(\mathbf{x}_i, \mathbf{x}_l) - d_M^2(\mathbf{x}_i, \mathbf{x}_j) \right) (\mathbf{X}_{il} - \mathbf{X}_{ij}) \\
& \frac{\partial}{\partial \mathbf{M}} (\mathbf{x}_l - \mathbf{x}_j)^T \mathbf{M} \mathbf{A}_0^{-1} \mathbf{M} (\mathbf{x}_l - \mathbf{x}_j) \\
&= \frac{\partial}{\partial \mathbf{M}} \text{tr}(\mathbf{X}_{jl} \mathbf{M} \mathbf{A}_0^{-1} \mathbf{M}) \\
&= \mathbf{X}_{jl} \mathbf{M} \mathbf{A}_0^{-1} + \mathbf{A}_0^{-1} \mathbf{M} \mathbf{X}_{jl} \\
& \frac{\partial}{\partial \mathbf{M}} \frac{(d_M^2(\mathbf{x}_i, \mathbf{x}_l) - d_M^2(\mathbf{x}_i, \mathbf{x}_j))^2}{4 \left((\mathbf{x}_l - \mathbf{x}_j)^T \mathbf{M} \mathbf{A}_0^{-1} \mathbf{M} (\mathbf{x}_l - \mathbf{x}_j) + \epsilon \right)} \\
&= \frac{2 \left(d_M^2(\mathbf{x}_i, \mathbf{x}_l) - d_M^2(\mathbf{x}_i, \mathbf{x}_j) \right) (\mathbf{X}_{il} - \mathbf{X}_{ij})}{4 \left((\mathbf{x}_l - \mathbf{x}_j)^T \mathbf{M} \mathbf{A}_0^{-1} \mathbf{M} (\mathbf{x}_l - \mathbf{x}_j) + \epsilon \right)} \\
&\quad - \frac{(d_M^2(\mathbf{x}_i, \mathbf{x}_l) - d_M^2(\mathbf{x}_i, \mathbf{x}_j))^2 (\mathbf{X}_{jl} \mathbf{M} \mathbf{A}_0^{-1} + \mathbf{A}_0^{-1} \mathbf{M} \mathbf{X}_{jl})}{4 \left((\mathbf{x}_l - \mathbf{x}_j)^T \mathbf{M} \mathbf{A}_0^{-1} \mathbf{M} (\mathbf{x}_l - \mathbf{x}_j) + \epsilon \right)^2},
\end{aligned}$$

where $\text{tr}(\cdot)$ denotes the trace operator. $\mathbf{X}_{ij} = (\mathbf{x}_i - \mathbf{x}_j)(\mathbf{x}_i - \mathbf{x}_j)^T$ and $\mathbf{X}_{il}, \mathbf{X}_{jl}$ are defined similarly. Substituting $\mathbf{A}_0 = \mathbf{I}$ gives Eq. 6.

B.1 Extension for high-dimensional Data

Support point, adversarial margin and gradient of the perturbation loss with dimensionality reduction are derived by following the same principle as in Appendix B.

The method of Lagrangian multiplier is applied to derive a closed-form solution to the support point:

$$\begin{aligned} & \min_{\mathbf{x}'_i} \left(\mathbf{A}^T (\mathbf{x}'_i - \mathbf{x}_i) \right)^T \left(\mathbf{A}^T (\mathbf{x}'_i - \mathbf{x}_i) \right) - \lambda \left(\mathbf{x}'_i - \frac{\mathbf{x}_j + \mathbf{x}_l}{2} \right)^T \mathbf{D}^T \mathbf{L}^T \mathbf{L} \mathbf{D} (\mathbf{x}_l - \mathbf{x}_j) \\ \frac{\delta}{\delta \mathbf{x}'_i} : \mathbf{x}'_i &= \mathbf{x}_i + \frac{\lambda}{2} \mathbf{A}_0^{-1} \mathbf{D}^T \mathbf{L}^T \mathbf{L} \mathbf{D} (\mathbf{x}_l - \mathbf{x}_j) \\ \frac{\lambda}{2} &= \frac{\left(\frac{\mathbf{x}_j + \mathbf{x}_l}{2} - \mathbf{x}_i \right)^T \mathbf{D}^T \mathbf{L}^T \mathbf{L} \mathbf{D} (\mathbf{x}_l - \mathbf{x}_j)}{(\mathbf{x}_l - \mathbf{x}_j)^T \mathbf{D}^T \mathbf{L}^T \mathbf{L} \mathbf{D} \mathbf{A}_0^{-1} \mathbf{D}^T \mathbf{L}^T \mathbf{L} \mathbf{D} (\mathbf{x}_l - \mathbf{x}_j)} \\ \mathbf{x}_{i,\min}^{\text{PCA}} &= \mathbf{x}_i + \frac{\left(\frac{\mathbf{x}_j + \mathbf{x}_l}{2} - \tilde{\mathbf{x}}_i \right)^T \mathbf{M} (\tilde{\mathbf{x}}_l - \tilde{\mathbf{x}}_j)}{(\tilde{\mathbf{x}}_l - \tilde{\mathbf{x}}_j)^T \mathbf{M} \mathbf{D} \mathbf{A}_0^{-1} \mathbf{D}^T \mathbf{M} (\tilde{\mathbf{x}}_l - \tilde{\mathbf{x}}_j)} \mathbf{A}_0^{-1} \mathbf{D}^T \mathbf{M} (\tilde{\mathbf{x}}_l - \tilde{\mathbf{x}}_j), \end{aligned}$$

where $\tilde{\mathbf{x}}$ denotes $\mathbf{D}\mathbf{x}$.

The squared adversarial margin is calculated from the definition of the hyperellipsoid:

$$\begin{aligned} r^2 &= (\mathbf{x}_i - \mathbf{x}_{\min}^{\text{PCA}})^T \mathbf{A}_0 (\mathbf{x}_i - \mathbf{x}_{\min}^{\text{PCA}}) \\ &= \frac{\left(d_M^2(\tilde{\mathbf{x}}_i, \tilde{\mathbf{x}}_l) - d_M^2(\tilde{\mathbf{x}}_i, \tilde{\mathbf{x}}_j) \right)^2}{4 \left((\tilde{\mathbf{x}}_l - \tilde{\mathbf{x}}_j)^T \mathbf{L}^T \mathbf{L} \mathbf{D} \mathbf{A}_0^{-1} \mathbf{D}^T \mathbf{L}^T \mathbf{L} (\tilde{\mathbf{x}}_l - \tilde{\mathbf{x}}_j) \right)^2} (\tilde{\mathbf{x}}_l - \tilde{\mathbf{x}}_j)^T \mathbf{L}^T \mathbf{L} \mathbf{D} \mathbf{A}_0^{-1} \mathbf{A}_0 \mathbf{A}_0^{-1} \mathbf{D}^T \mathbf{L}^T \mathbf{L} (\tilde{\mathbf{x}}_l - \tilde{\mathbf{x}}_j) \\ &= \frac{\left(d_M^2(\tilde{\mathbf{x}}_i, \tilde{\mathbf{x}}_l) - d_M^2(\tilde{\mathbf{x}}_i, \tilde{\mathbf{x}}_j) \right)^2}{4 (\tilde{\mathbf{x}}_l - \tilde{\mathbf{x}}_j)^T \mathbf{M} \mathbf{D} \mathbf{A}_0^{-1} \mathbf{D}^T \mathbf{M} (\tilde{\mathbf{x}}_l - \tilde{\mathbf{x}}_j)} \end{aligned}$$

The perturbation loss is defined similarly to Eq. 4 as follows:

$$J_{\text{P}}^{\text{PCA}} = \frac{1}{|\mathcal{R}|} \sum_{\mathcal{R}} \left\{ [\tau^2 - \tilde{d}_{\mathbf{E}}^2(\mathbf{x}_i, \mathbf{x}_{i,\min}^{\text{PCA}})]_+ \mathbb{1}_{\{d_M^2(\tilde{\mathbf{x}}_i, \tilde{\mathbf{x}}_l) > d_M^2(\tilde{\mathbf{x}}_i, \tilde{\mathbf{x}}_j)\}} + \tau^2 \mathbb{1}_{\{d_M^2(\tilde{\mathbf{x}}_i, \tilde{\mathbf{x}}_l) \leq d_M^2(\tilde{\mathbf{x}}_i, \tilde{\mathbf{x}}_j)\}} \right\}.$$

The gradient of $J_{\text{P}}^{\text{PCA}}$ is given as:

$$\begin{aligned} \frac{\partial J_{\text{P}}^{\text{PCA}}}{\partial \mathbf{M}} &= \frac{1}{|\mathcal{R}|} \sum_{\mathcal{R}} \alpha_{ijl} \left\{ \frac{\left(d_M^2(\tilde{\mathbf{x}}_i, \tilde{\mathbf{x}}_l) - d_M^2(\tilde{\mathbf{x}}_i, \tilde{\mathbf{x}}_j) \right) (\tilde{\mathbf{X}}_{ij} - \tilde{\mathbf{X}}_{il})}{2 \left((\tilde{\mathbf{x}}_l - \tilde{\mathbf{x}}_j)^T \mathbf{M} \mathbf{D} \mathbf{A}_0^{-1} \mathbf{D}^T \mathbf{M} (\tilde{\mathbf{x}}_l - \tilde{\mathbf{x}}_j) + \epsilon \right)} \right. \\ &\quad \left. + \frac{\left(d_M^2(\tilde{\mathbf{x}}_i, \tilde{\mathbf{x}}_l) - d_M^2(\tilde{\mathbf{x}}_i, \tilde{\mathbf{x}}_j) \right)^2}{4 \left((\tilde{\mathbf{x}}_l - \tilde{\mathbf{x}}_j)^T \mathbf{M} \mathbf{D} \mathbf{A}_0^{-1} \mathbf{D}^T \mathbf{M} (\tilde{\mathbf{x}}_l - \tilde{\mathbf{x}}_j) + \epsilon \right)^2} (\tilde{\mathbf{X}}_{jl} \mathbf{M} \mathbf{D} \mathbf{A}_0^{-1} \mathbf{D}^T + \mathbf{D} \mathbf{A}_0^{-1} \mathbf{D}^T \mathbf{M} \tilde{\mathbf{X}}_{jl}) \right\}. \end{aligned}$$

C Sparse compositional metric learning with certified robustness

We start by briefly revisiting the sparse compositional metric learning (SCML) method [31]. The core idea is to represent the Mahalanobis distance as a non-negative combination of K basis elements; that is,

$$\mathbf{M} = \sum_{k=1}^K w_k \mathbf{b}_k \mathbf{b}_k^T, \quad \mathbf{w} \geq 0,$$

where the basis set $\{\mathbf{b}_k\}_{k=1}^K$ is generated by using the Fisher discriminative analysis at several local regions. To learn a discriminative metric with good generalization ability, the learning objective comprises a margin-based hinge loss function and an L_1 -norm regularization term as follows:

$$\min_{\mathbf{w}} J_{\text{SCML}} = \frac{1}{|\mathcal{R}|} \sum_{\mathcal{R}} [1 + d_{\mathbf{w}}^2(\mathbf{x}_i, \mathbf{x}_j) - d_{\mathbf{w}}^2(\mathbf{x}_i, \mathbf{x}_l)]_+ + \eta \|\mathbf{w}\|_1,$$

where $\eta \geq 0$ controls the degree of sparsity.

Similar to LMNN-CR, we propose SCML with certified robustness (SCML-CR) by adding the perturbation loss J_{P} (Eq. 4) to the original objective function J_{SCML} :

$$\min_{\mathbf{M} \in \mathbb{S}_+^p} J = J_{\text{SCML}} + \lambda J_{\text{P}}. \quad (8)$$

The adversarial margin of Eq. 3 is now a function of \mathbf{w} :

$$\begin{aligned} d_{\mathbf{E}}^2(\mathbf{x}_i, \mathbf{x}_{i,\min}) &= \frac{(d_{\mathbf{w}}^2(\mathbf{x}_i, \mathbf{x}_l) - d_{\mathbf{w}}^2(\mathbf{x}_i, \mathbf{x}_j))^2}{4d_{\mathbf{w}^2}^2(\mathbf{x}_j, \mathbf{x}_l)} \\ d_{\mathbf{w}}^2(\mathbf{x}_i, \mathbf{x}_j) &= (\mathbf{x}_i - \mathbf{x}_j)^T \left(\sum_{k=1}^K w_k \mathbf{b}_k \mathbf{b}_k^T \right) (\mathbf{x}_i - \mathbf{x}_j) \\ d_{\mathbf{w}^2}^2(\mathbf{x}_j, \mathbf{x}_l) &= (\mathbf{x}_j - \mathbf{x}_l)^T \left(\sum_{k_1=1}^K \sum_{k_2=1}^K w_{k_1} w_{k_2} \mathbf{b}_{k_1} \mathbf{b}_{k_1}^T \mathbf{b}_{k_2} \mathbf{b}_{k_2}^T \right) (\mathbf{x}_j - \mathbf{x}_l). \end{aligned}$$

The optimization problem (Eq. 8) is solved via the accelerated proximal gradient descent algorithm. The gradient of $J_{\mathcal{P}}$ with respect to \mathbf{w} is as follows:

$$\begin{aligned} \frac{\partial J_{\mathcal{P}}}{\partial w_k} &= \frac{1}{|\mathcal{R}|} \sum_{\mathcal{R}} \alpha_{ijl} \left\{ \frac{d_{\mathbf{M}}^2(\mathbf{x}_i, \mathbf{x}_l) - d_{\mathbf{M}}^2(\mathbf{x}_i, \mathbf{x}_j)}{2(d_{\mathbf{M}^2}^2(\mathbf{x}_j, \mathbf{x}_l) + \epsilon)} \text{tr} \left(\mathbf{b}_k \mathbf{b}_k^T (\mathbf{X}_{ij} - \mathbf{X}_{il}) \right) \right. \\ &\quad \left. + \frac{[d_{\mathbf{M}}^2(\mathbf{x}_i, \mathbf{x}_l) - d_{\mathbf{M}}^2(\mathbf{x}_i, \mathbf{x}_j)]^2}{4(d_{\mathbf{M}^2}^2(\mathbf{x}_j, \mathbf{x}_l) + \epsilon)^2} \text{tr} \left((\mathbf{b}_k \mathbf{b}_k^T \mathbf{M} + \mathbf{M} \mathbf{b}_k \mathbf{b}_k^T) \mathbf{X}_{jl} \right) \right\}, \end{aligned}$$

where ϵ is a small constant added to the denominator of $d_{\mathbf{E}}^2(\mathbf{x}_i, \mathbf{x}_{i,\min})$.

D Preliminaries and theorem on generalization benefit

D.1 Preliminaries

Definition 1. [2] An algorithm \mathcal{A} is $(K, \epsilon(\cdot), \hat{n}(\cdot))$ pseudo-robust for $K \in \mathbb{N}$, $\epsilon(\cdot) : (\mathcal{Z} \times \mathcal{Z} \times \mathcal{Z})^n \rightarrow \mathbb{R}$ and $\hat{n}(\cdot) : (\mathcal{Z} \times \mathcal{Z} \times \mathcal{Z})^n \rightarrow \{1, \dots, n^3\}$ if $\mathcal{Z} = (\mathcal{X} \times \mathcal{Y})$ can be partitioned into K disjoint sets, denoted by $\{C_k\}_{k=1}^K$, such that for all training samples $\mathbf{s} \in \mathcal{Z}^n$ drawn independently and identically distributed (IID) from the probability distribution \mathcal{P} , there exists a subset of training triplets $\hat{t}_{\mathbf{s}} \subseteq t_{\mathbf{s}}$, with $|\hat{t}_{\mathbf{s}}| = \hat{n}(t_{\mathbf{s}})$, such that the following holds: $\forall (\mathbf{s}_1, \mathbf{s}_2, \mathbf{s}_3) \in \hat{t}_{\mathbf{s}}, \forall \mathbf{z}_1, \mathbf{z}_2, \mathbf{z}_3 \in \mathcal{Z}, \forall i, j, l = 1, \dots, K$, if $\mathbf{s}_1, \mathbf{z}_1 \in C_i, \mathbf{s}_2, \mathbf{z}_2 \in C_j$ and $\mathbf{s}_3, \mathbf{z}_3 \in C_l$, then

$$|\ell(\mathcal{A}_{t_{\mathbf{s}}}, \mathbf{s}_1, \mathbf{s}_2, \mathbf{s}_3) - \ell(\mathcal{A}_{t_{\mathbf{s}}}, \mathbf{z}_1, \mathbf{z}_2, \mathbf{z}_3)| \leq \epsilon(t_{\mathbf{s}}).$$

Theorem 2. [2] If \mathcal{A} is $(K, \epsilon(\cdot), \hat{n}(\cdot))$ pseudo-robust and the training triplets $t_{\mathbf{s}}$ come from a sample generated by n IID draws from \mathcal{P} , then for any $\delta > 0$, with probability at least $1 - \delta$ we have:

$$|\mathcal{L}(\mathcal{A}_{t_{\mathbf{s}}}) - \ell_{emp}(\mathcal{A}_{t_{\mathbf{s}}})| \leq \frac{\hat{n}(t_{\mathbf{s}})}{n^3} \epsilon(t_{\mathbf{s}}) + B \left(\frac{n^3 - \hat{n}(t_{\mathbf{s}})}{n^3} + 3 \sqrt{\frac{2K \ln 2 + 2 \ln 1/\delta}{n}} \right), \quad (9)$$

where B is a constant denoting the upper bound of the loss function ℓ .

Definition 2. [36] A δ -cover of a set Θ with respect to a metric ρ is a set $\{\theta^1, \dots, \theta^N\} \subset \Theta$ such that for each $\theta \in \Theta$, there exists some $i \in \{1, \dots, N\}$ such that $\rho(\theta, \theta^i) \leq \delta$. The δ -covering number $N(\delta, \Theta, \rho)$ is the cardinality of the smallest δ -cover.

D.2 Theorem and proof

Theorem 3. Let \mathbf{M}^* be the optimal solution to Eq. 5. Then for any $\delta > 0$, with probability at least $1 - \delta$ we have:

$$|\mathcal{L}(\mathbf{M}^*) - \ell_{emp}(\mathbf{M}^*)| \leq \frac{\hat{n}(t_{\mathbf{s}})}{n^3} + B \left(\frac{n^3 - \hat{n}(t_{\mathbf{s}})}{n^3} + 3 \sqrt{\frac{2K \ln 2 + 2 \ln 1/\delta}{n}} \right),$$

where $\hat{n}(t_{\mathbf{s}})$ denotes the number of triplets whose adversarial margins are larger than τ , B is a constant denoting the upper bound of the loss function (i.e. Eq. 5), and $K = |\mathcal{Y}|(1 + \frac{2}{\tau})^p$.

Proof. After embedding the perturbation loss, learning algorithms that minimize the classical triplet loss, i.e. $[1 + d_{\mathbf{M}}^2(\mathbf{x}_i, \mathbf{x}_j) - d_{\mathbf{M}}^2(\mathbf{x}_i, \mathbf{x}_l)]_+ \cdot \mathbf{1}_{\{y_i=y_j \neq y_l\}}$, are $(|\mathcal{Y}|(1 + \frac{2}{\tau})^p, 1, \hat{n}(\cdot; \tau))$ pseudo-robust. $\epsilon = 1$ since, by definition of certified neighborhood, any \mathbf{x} that falls into the Euclidean ball with center \mathbf{x}_i and a radius of the desired margin τ will satisfy $d_{\mathbf{M}}^2(\mathbf{x}, \mathbf{x}_l) > d_{\mathbf{M}}^2(\mathbf{x}, \mathbf{x}_j)$, hence any change in loss is bounded by 1. The value of K can be determined via the covering number [2]. The instance space \mathcal{X} can be partitioned by using the covering number $N(\tau, \mathcal{X}, \|\cdot\|_2)$. By normalizing all instances to have unit L_2 -norm, we obtain a finite covering number as $N \leq (1 + \frac{2}{\tau})^p$ [36]. The label space \mathcal{Y} can be partitioned into $|\mathcal{Y}|$ sets. Therefore, the number of disjoint sets, i.e. K , is always smaller than $|\mathcal{Y}|(1 + \frac{2}{\tau})^p$. \square

E Experimental setup and results

E.1 Datasets

Table 6 lists information on sample size, feature dimension and class information.

Table 6: Characteristics of the datasets.

dataset	# instances (training,test)	# features (reduced dimensions)	# classes	# rounds
UCI data				
Australian	690	14	2	20
Breast cancer	683	9	2	20
Fourclass	862	2	2	20
Haberman	306	3	2	20
Iris	150	4	3	20
Segment	2310	19	7	20
Sonar	208	60	2	20
Voting	435	16	2	20
WDBC	569	30	2	20
Wine	178	13	3	20
High-dimensional data				
Isolet	7797 (1560,1558)	617 (170)	26	4
MNIST	4000 (2000,2000)	784 (141)	10	1

E.2 Experimental setting

Hyperparameter tuning of compared methods LMNN, SCML, DRIFT and AML are implemented by using the official codes provided by the authors; all parameters are set as default apart from the trade-off parameter. Trade-off parameters are tuned via five-fold cross-validation on the training data. For LMNN, the trade-off parameter μ is chosen from $\{0.1, 0.2, \dots, 0.9\}$. For SCML, the weight of the regularization term η is chosen from $\{10^{-5}, 10^{-4}, \dots, 10^3\}$, and the number of bases is set as 200, 400 and 1000 for UCI datasets whose sample size is smaller than 500, larger than 500, and high-dimensional datasets, respectively. For LDD, the regularizer weight is chosen from $\{10^{-6}, \dots, 10^2\}$. For CAP, the regularizer weight is chosen from $\{10^{-3}, \dots, 10\}$, and the rank of \mathbf{M} is chosen from 10 values equally spaced between 1 and p . For DRIFT and AML, we search the grid suggested by the authors.

Experimental setting of LMNN-CR We first explain the ranges of hyperparameters, i.e. $\tau \in U(0, P_{90\%}\{d_{\mathbf{E}}(\mathbf{x}_i, \mathbf{x}_{i,\min})\})$, $\lambda \in U(0, 4/\tau^2)$. Setting the upper bound of the adversarial margin τ via the percentile avoids unnecessary large values, matching our intention to expand the certified neighborhood primarily for hard instances. The upper bound of the weight parameter λ depends on the realization of τ to ensure that magnitudes of perturbation loss and LMNN loss are at the same level. \mathbf{M} is initialized as the identity matrix. The learning rate γ is initialized to 1. Following [39]’s work, γ is increased by 1% if the loss function decreases and decreased by 50% otherwise. The training stops if the relative change in the objective function is smaller than the threshold of 1e-7 or reaches the maximum number of iterations of 1000.

Experimental setting of SCML-CR SCML-CR is tuned in the same manner as LMNN-CR; the range of η and the number of bases are same as SCML, and the ranges of τ and λ are same as LMNN-CR. The method is optimized via the accelerated proximal gradient descent algorithm with a backtracking stepsize rule [35]. The initial learning rate is set as 1 and the shrinkage factor is set as 0.8. \mathbf{w} is initialized as the unit vector.

E.3 Comparisons between LMNN and LMNN-CR

In this section, we provide three toy examples to illustrate the difference between LMNN and LMNN-CR.

The first example visualizes the effect of the perturbation loss on the adversarial margin. The dataset includes two classes of ten instances each, simulated from Gaussian distributions. The mean vectors of the positive and negative classes are set as $[0.4, 0.4]$ and $[-0.4, -0.4]$ respectively, and the covariance matrices for both classes are set as $[1, -0.5; -0.5, 1]$. Mean centering and standardization are performed prior to metric learning. In Fig. 4, we plot the adversarial margins of training instances after learning the Mahalanobis distance via LMNN or LMNN-CR; that is, $d_{\mathbf{E}}(\mathbf{x}_i, \mathbf{x}_{\min})$ calculated with respect to different \mathbf{M} . For clarity, the margin size is shrunk by 70 percent of its original size for all instances. For easy instances whose nearest neighbors are instances of the same class (e.g. A), incorporating the perturbation loss enlarges the margin by a large magnitude. For hard instances which are located close to instances of the opposite class (e.g. B), the margin still gets enlarged although to a less extent. For instances whose margin is already quite large under LMNN (e.g. C), LMNN-CR may not further enlarge their margins, and even shrink the margins in some cases, which agrees with the design of the desired margin τ .

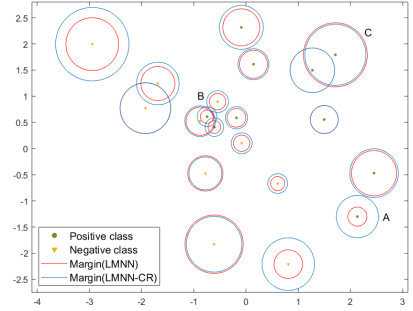


Figure 4: Visualization and comparison of adversarial margins of LMNN (without) and LMNN-CR (with the perturbation loss).

The second and third examples illustrate the difference in the learning mechanisms of LMNN and LMNN-CR. In the second example, we simulate a two-dimensional binary classification dataset, as shown in Fig. 5a. The positive class includes 100 instances drawn uniformly from $[-3, 0]$ in the horizontal (abbr. 1st) direction and $[0, 1]$ in the vertical (abbr. 2nd) direction. The negative class consists of two clusters, where the first cluster includes 100 instances drawn from $U(-3, 0)$ and $U(-0.6, -0.5)$ in the 1st and 2nd directions respectively, and the second cluster includes 20 instances drawn from $U(0, 0.1)$ and $U(0, 1)$ in the two directions respectively. By design, instances of positive and negative classes can be separated in both directions, while the separability in the 1st direction is much smaller than the 2nd direction. Figs. 5b, 5c show the instances in the projected feature space with metrics learned from LMNN and LMNN-CR, respectively; the projection direction is indicated by the unit vector of red and blue lines; and the metric and the average of adversarial margins ($\bar{d}_{\mathbf{E}}(\mathbf{x}_i, \mathbf{x}_{i,\min})$) are given in the caption. The objective of LMNN is to satisfy the distance margin. Thus, it expands the distance in both directions. Moreover, since the 1st direction has a small separability in the original instance space, this direction is assigned with a larger weight. In contrast, LMNN-CR controls the scale of \mathbf{M} . Moreover, a notable difference is that the 2nd direction is assigned with a larger weight than the 1st direction, which is again caused by the small separability in the 1st direction. As any perturbation in the 1st direction is highly likely to result in a misclassification, our method diverts more attention to robust features, i.e. the 2nd direction.

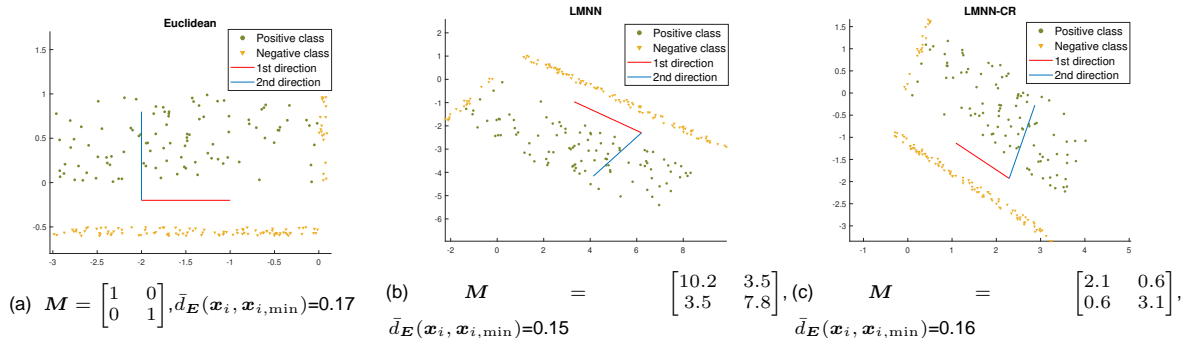


Figure 5: Comparison of learning mechanisms of LMNN and LMNN-CR when features exhibit different separability.

In the third example, we simulate a three-dimensional binary classification dataset, as shown in Fig. 6a. The positive and negative classes each include 100 instances. The first two dimensions are drawn from multivariate Gaussian distributions with $\boldsymbol{\mu}_p = [0.45, 0.45]$, $\boldsymbol{\mu}_n = [-0.45, -0.45]$, $\boldsymbol{\Sigma}_p = \boldsymbol{\Sigma}_n = \begin{bmatrix} 1 & -0.9 \\ -0.9 & 1 \end{bmatrix}$. The third dimension equals the sum of the first two dimensions, plus white Gaussian noise with standard deviation of 0.01. By design, the dataset exhibits the problem of strong multicollinearity. This issue has little influence on LMNN as the data is nearly separable in all directions. However, it will affect

the certified neighborhood. Specifically, if the metric assigns equal weights to all dimensions, then the perturbation should be small in all directions so as to guarantee that the perturbed instance stays on the correct side of the decision boundary. In contrast, if the metric assigns weights only to the third dimension, then the perturbation in the first two dimensions will not cause any change in the learned feature space and hence a larger magnitude of perturbation in the third dimension could be allowed. This expectation is supported by the empirical result in Fig. 6c, where the distance in the third dimension is more important than the first two dimensions.

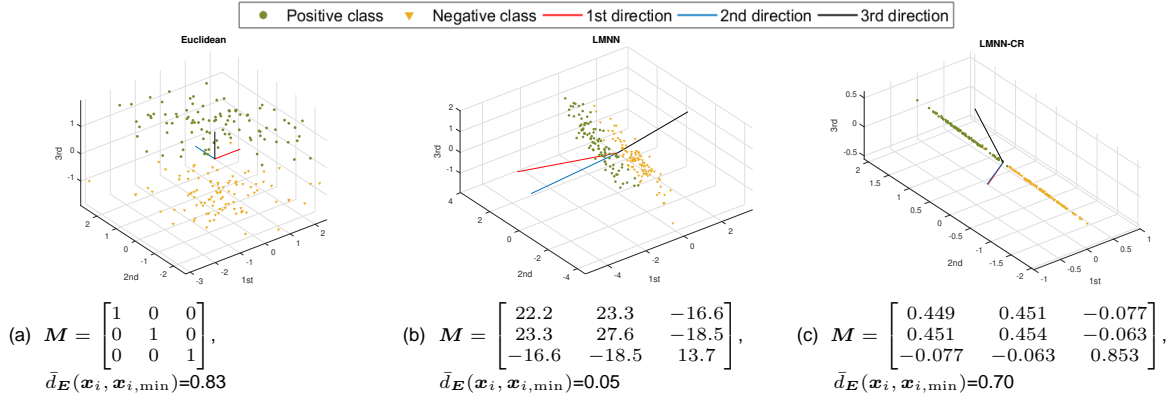


Figure 6: Comparison of learning mechanisms of LMNN and LMNN-CR when confronting the problem of multicollinearity.

In summary, our method learns a discriminative metric, and meanwhile, imposes a data-dependent regularization on the metric. It also achieves larger adversarial margins than LMNN.

E.4 Additional experimental results

Table 7 is a supplement to Sec. 3.1.3, which reports the robustness of DML methods under spherical Gaussian noise with the SNR of 5 dB.

Table 7: Classification accuracy of DML Methods on noise-contaminated datasets. Spherical Gaussian noise with an SNR of 5 dB is added to test data.

Dataset	AML	LMNN-based					SCML-based	
		LMNN	LDD	CAP	DRIFT	LMNN-CR	SCML	SCML-CR
Australian	82.67 ± 1.59	82.46 ± 1.58	83.02 ± 1.58	82.36 ± 1.56	82.58 ± 1.45	83.50 ± 1.56	82.93 ± 1.65	83.42 ± 1.68
Breast cancer	96.74 ± 1.01	96.25 ± 1.09	96.69 ± 1.09	96.35 ± 1.02	96.66 ± 1.00	96.71 ± 1.08	96.40 ± 1.05	96.65 ± 1.06
Fourclass	68.91 ± 1.16	67.62 ± 1.23	68.77 ± 1.14	67.63 ± 1.12	69.03 ± 1.13	69.01 ± 1.17	68.07 ± 1.16	68.86 ± 1.06
Haberman	69.81 ± 1.85	69.84 ± 1.79	69.92 ± 1.87	69.23 ± 2.00	69.09 ± 2.49	69.89 ± 1.90	69.65 ± 1.63	69.88 ± 1.83
Iris	78.92 ± 3.25	78.61 ± 2.97	78.87 ± 3.16	77.79 ± 3.27	78.43 ± 3.09	79.04 ± 3.09	78.16 ± 3.58	79.01 ± 3.12
Segment	87.92 ± 0.69	81.02 ± 3.55	86.15 ± 1.26	85.34 ± 2.47	86.63 ± 1.09	84.72 ± 2.62	60.18 ± 9.73	61.33 ± 9.05
Sonar	83.46 ± 3.39	83.56 ± 4.27	86.18 ± 2.95	85.41 ± 2.82	84.65 ± 3.30	85.00 ± 3.15	77.01 ± 4.23	79.49 ± 3.80
Voting	94.10 ± 1.07	94.00 ± 1.00	94.25 ± 1.14	94.37 ± 1.17	93.95 ± 1.12	94.64 ± 1.21	93.99 ± 1.15	94.64 ± 1.09
WDBC	96.49 ± 1.12	91.71 ± 1.90	96.30 ± 0.94	96.16 ± 1.08	96.04 ± 0.86	96.11 ± 0.88	95.74 ± 1.30	96.21 ± 1.16
Wine	95.12 ± 1.12	93.33 ± 1.63	94.03 ± 1.39	93.97 ± 1.47	94.66 ± 1.15	94.51 ± 1.20	94.01 ± 1.56	94.61 ± 1.32
# outperform	-	10	6	7	7	-	10	-

Table 8 is a supplement to Table 3 of the main text, which reports the performance of AML, LDD and DRIFT on high-dimensional datasets.

E.5 Parameter sensitivity

The proposed LMNN-CR includes three hyperparameters – μ for the weight of similarity constraints, λ for the weight of the perturbation loss, and τ for the desired adversarial margin. We investigate their influences on the classification performance by varying one hyperparameter and fixing the other two at their optimal values. Fig. 7 shows the accuracy on MNIST evaluated over the range of the hyperparameter. The performance changes smoothly with respect to μ . It is stable over a wide range of λ . When λ equals

Table 8: Generalization and robustness of additional DML methods on high-dimensional datasets.

Method	Isolet						MNIST					
	Clean	SG-20 (0.081)	SG-5 (0.423)	G-20 (0.059)	G-5 (0.318)	Adv. margin	Clean	SG-20 (0.054)	SG-5 (0.294)	G-20 (0.065)	G-5 (0.348)	Adv. margin
AML	86.8 ±3.2	86.6 ±3.5	86.0 ±3.7	86.7 ±3.6	86.2 ±3.8	0.126	89.3	88.7	88.9	89.3	89.2	0.214
LDD	90.9 ±3.9	90.8 ±4.1	88.0 ±3.8	90.7 ±4.1	89.1 ±4.1	0.133	90.9	90.9	90.8	91.0	90.3	0.223
DRIFT			NA				90.9	90.8	87.5	90.7	89.5	0.205

DRIFT is unable to learn a metric on Isolet and hence is not reported.

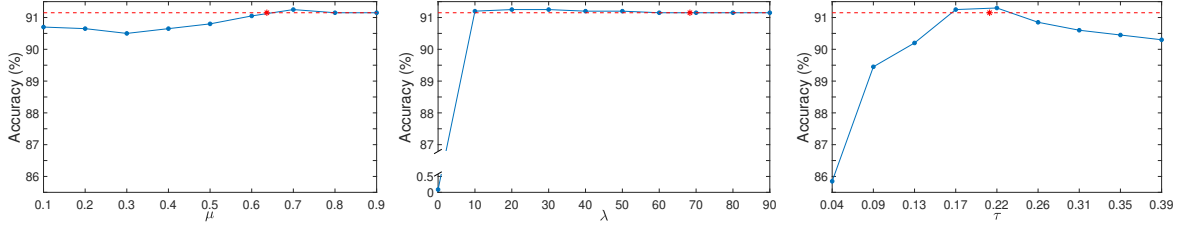


Figure 7: Sensitivity of LMNN-CR to hyperparameters (indicated by the straight line). The optimal accuracy and parameter value found via CV are indicated by the dashed line and asterisk, respectively.

0, LMNN-CR fails to learn a metric and returns a zero matrix. The performance is most affected by τ . Indeed, τ plays the central role in LMNN-CR as it determines the distribution of adversarial margins. Therefore, we shall strive to search for its optimal value.